

Article

Purification and Structural Characterization of the Auxiliary Activity 9 Native Lytic Polysaccharide Monooxygenase from *Thermoascus aurantiacus* and Identification of Its C1- and C4-Oxidized Reaction Products

Weishuai Yu ^{1,†} , Imran Mohsin ^{2,3,†} , Anastassios C. Papageorgiou ^{2,3,*}  and Duochuan Li ^{1,*}¹ Department of Mycology, Shandong Agricultural University, Taian 271018, China; y2020010096@163.com² Turku Bioscience Centre, University of Turku, 20521 Turku, Finland; mohsin.imran@utu.fi³ Turku Bioscience Centre, Åbo Akademi University, 20521 Turku, Finland

* Correspondence: anapap@utu.fi (A.C.P.); lidc20@sdau.edu.cn (D.L.)

† These authors contributed equally to this work.

Abstract: Auxiliary activity 9 (AA9) lytic polysaccharide monooxygenases (LPMOs) are copper-dependent oxidoreductases that use O₂ or H₂O₂ to perform oxidative cleavage of cellulose in the presence of an electron donor. Combined with cellulases, they can assist in a more efficient cleavage of cellulose. AA9 LPMOs have therefore attracted considerable attention in recent years for use in biotechnological applications. Here, a native AA9 LPMO (nTaAA9A) from the thermophilic fungus *Thermoascus aurantiacus* was purified and characterized. The enzyme was shown to be active and able to cleave cellulose and xylan to produce C1- and C4-oxidized products. It was also found to retain about 84.3, 63.7, and 35.3% of its activity after incubation for 30 min at 60, 70, and 80 °C, respectively, using quantitative activity determination. The structure was determined to 1.36 Å resolution and compared with that of the recombinant enzyme expressed in *Aspergillus oryzae*. Structural differences in the glycosylated Asn138 and in solvent-exposed loops were identified.

Keywords: monooxygenase; oxidoreductase; copper; cellulose degradation; thermostability; thermophilic fungus



Citation: Yu, W.; Mohsin, I.; Papageorgiou, A.C.; Li, D. Purification and Structural Characterization of the Auxiliary Activity 9 Native Lytic Polysaccharide Monooxygenase from *Thermoascus aurantiacus* and Identification of Its C1- and C4-Oxidized Reaction Products. *Catalysts* **2022**, *12*, 139. <https://doi.org/10.3390/catal12020139>

Academic Editors: Evangelos Topakas and Giovanni Gadda

Received: 22 November 2021

Accepted: 18 January 2022

Published: 23 January 2022

Publisher's Note: MDPI stays neutral with regard to jurisdictional claims in published maps and institutional affiliations.



Copyright: © 2022 by the authors. Licensee MDPI, Basel, Switzerland. This article is an open access article distributed under the terms and conditions of the Creative Commons Attribution (CC BY) license (<https://creativecommons.org/licenses/by/4.0/>).

1. Introduction

Cellulose is a polysaccharide consisting of a linear chain of glucose units connected through 1,4-β-glycosidic bonds. As the most abundant renewable organic compound on earth, cellulose can be turned into economically viable biofuels by enzymatic degradation [1]. A significant milestone in the enzymatic degradation of cellulose was the discovery of lytic polysaccharide monooxygenases (LPMOs) that catalyze the cleavage of 1,4-β-glycosidic bonds in cellulose. Contrary to cellulases which, as glycoside hydrolases (GHs), catalyze the breakage of 1,4-β-glycosidic bonds in cellulose via a hydrolytic mechanism, LPMOs follow an oxidative mechanism [2–4]. Extensive studies in LPMOs have led to their further classification as Auxiliary Activity (AA) enzymes in the Carbohydrate Active enZymes (CAZy; www.cazy.org; accessed on 20 November 2021) database [5], where they form eight separate families (AA9–AA11, AA13–AA17) [6,7]. LPMOs of fungal origin are found in the families AA9 (formerly GH61) and AA11.

The discovery of LPMOs has revolutionized the enzymatic degradation of cellulose because LPMOs can cleave crystalline cellulose and allow cellulases, which interact with single cellulose chains, to hydrolyze cellulose more efficiently [4,8,9]. Apart from cellulose degradation, LPMOs have also been suggested to play a role in various other biological processes, such as bacterial pathogenicity [10] and viral virulence [11].

LPMOs are copper-dependent oxidoreductases that employ O₂ or H₂O₂ to carry out oxidative cleavage of cellulose in the presence of an electron donor [4,8,9,12–15]. LPMOs

use a cellulose degradation mechanism different from that of cellulases, as they lack a conserved carboxylate pair and an active site groove [16]. The reaction proceeds through an oxidative step that involves the hydroxylation of crystalline cellulose at the C1 or C4 carbon, leading to the subsequent cleavage of the glycosidic bond.

Crystal structures of ~30 LPMOs are currently known [16], including those of *Thermoascus aurantiacus* TaAA9A (PDB id 2yet) [17], *Aspergillus fumigatus* AfuAA9A (PDB id 6h1z) [18], *Serratia marcescens* SmAA10A (PDB id 2bem) [19], *Aspergillus oryzae* AoAA13 (PDB id 4opb) [20], and recently, McAA9F (PDB id 7ntl) [21] from the thermophilic fungus *Malbranchea cinnamomea*. The available LPMO structures have revealed a planar surface suitable for binding crystalline cellulose and the presence of a single copper ion located at the center of the planar surface [4,12]. A remarkable catalytic characteristic of LPMOs is the difference in regioselectivity of cellulose oxidative cleavage. It has been shown that LPMOs are able to cleave cellulose by C1 and C4 oxidation to form non-oxidized and oxidized cello-oligosaccharides [17,22,23].

LPMOs are also capable of breaking down xylan. Fungal AA9 LPMOs, such as LsAA9A from *Lentinus similis* [12] and MtLPMO9A from *Myceliophthora thermophila* [24] have been shown to cleave xylan. Xylan-active AA14 LPMO from *Pycnoporus coccineus*, PcAA14B, and GH30 TtXyn30A from *Thermothelomyces thermophila* were found to act synergistically with a family GH11 endoxylanase (AnXyn11) in the degradation of xylan-containing substrates, resulting in an increase of the released total oligosaccharides [25]. A synergistic action of keratinases with LPMOs has also been proposed [26], thus offering additional strategies to improve keratinase performance.

Various protein engineering efforts have been carried out to improve activity and thermostability of LPMOs. For example, a tetramutant in AfAA9A_B with remarkable improvement in biomass conversion at elevated temperatures has been reported [18]. Genomic sequencing has shown a number of AA9 LPMOs in thermophilic fungi [27–29]. AA9 LPMOs from thermophilic fungi are potentially more thermostable than those from mesophilic fungi; thus, they have received increased attention in recent years [17,28]. The recombinant AA9 LPMO (rTaAA9A) from the thermophilic fungus *Thermoascus aurantiacus* is well characterized, and its C1- and C4-oxidized products were previously identified based on mass spectrometry analysis [17] and sequence and phylogenetic analysis [27]. Here, we report the purification and characterization of the native TaAA9A (nTaAA9A). The C1- and C4-oxidized products of nTaAA9A were identified, and the thermostability of the enzyme was studied using quantitative activity determination. nTaAA9A reaction products with xylan as a substrate were identified as well. Furthermore, its structure was determined and compared with that of the recombinant enzyme expressed in *Aspergillus oryzae*.

2. Results and Discussion

2.1. Purification

A native LPMO was purified to homogeneity from the culture filtrate of *T. aurantiacus* growing in cellulose-containing medium by ion-exchange chromatography and gel filtration (Figure 1a) and identified as TaAA9A using liquid chromatography–tandem mass spectrometry (LC–MS/MS) (Figure S1a,b). The molecular weight of the purified TaAA9A was estimated to be about 27.42 kDa by SDA-PAGE (Figure 1a), which is higher than that calculated based on the deduced amino acid sequence (24.39 kDa), suggesting glycosylation. Using NetNGlyc 1.0 Server (www.cbs.dtu.dk/services/NetNGlyc/ accessed on 20 November 2021), a putative N-linked glycosylation site (Asn138) in the deduced amino acid sequence of TaAA9A was predicted, indicating that the TaAA9A protein may be N-glycosylated. Further periodic acid–Schiff staining confirmed nTaAA9A's glycosylation (Figure 1b), in agreement with the predicted results of NetNGlyc 1.0 Server and SDS-PAGE analysis.

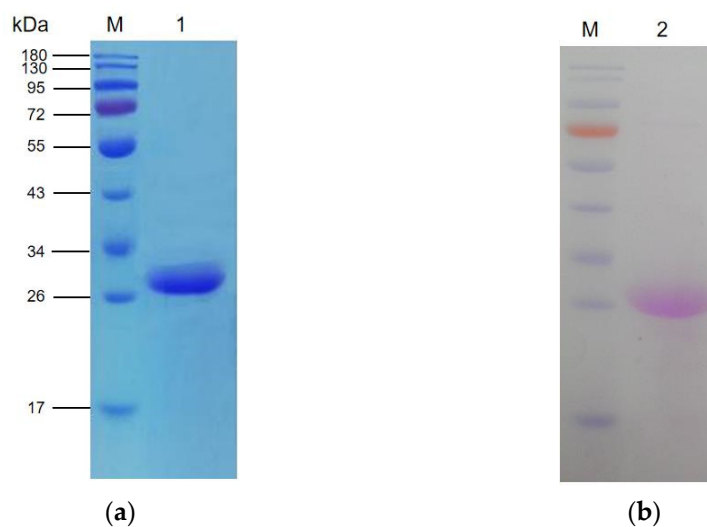


Figure 1. SDS-PAGE of the purified native *nTaAA9A*. *nTaAA9A* was visualized (a) by staining with Coomassie Brilliant Blue; (b) by staining with the Pierce™ Glycoprotein Staining Kit. Lane M, protein markers (kDa); Lanes 1 and 2, *nTaAA9A*.

2.2. Product Identification

nTaAA9A reaction products were identified using thin-layer chromatography (TLC), matrix-assisted laser desorption ionization–time-of-flight mass spectrometry (MALDI-TOF MS), and high-performance liquid chromatography–refractive index detector (HPLC-RID). TLC analysis showed that *nTaAA9A* can cleave cellulose to yield cello-oligosaccharides with various degrees of polymerization (DP) (Figure 2). To demonstrate the presence of C1- and C4-oxidized oligosaccharides, a previously described chemical method [17,30] using methyl iodide to permethylate *nTaAA9A* products was employed. As expected, molecular ion peaks at m/z DPn + 30 and m/z DPn – 16 corresponding to C1- and C4-oxidized oligosaccharides were observed using MALDI-TOF MS (Figure 3). To further determine the presence of C1- and C4-oxidized oligosaccharides, a chemical method using trifluoroacetic acid (TFA) to hydrolyze *nTaAA9A* products was applied. Using HPLC-RID analysis, two C1- and C4-oxidized monosaccharides were observed (Figure 4a,b). These results indicate the presence of C1- and C4-oxidized oligosaccharides in *nTaAA9A* reaction products.

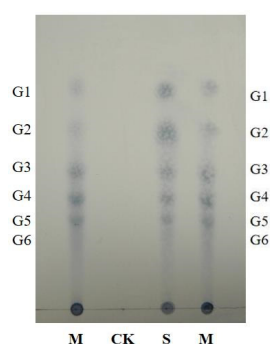


Figure 2. TLC analysis of *nTaAA9A* reaction products using PASC as a substrate. *nTaAA9A* reaction products were formed following incubation of 0.5% PASC with *nTaAA9A* in 10 mM HOAc-NH₄OAc (pH 5.0) and 1 mM ascorbate at 50 °C for 48 h. Lane M, standard cello-oligosaccharides (G1–G6); Lane S, *nTaAA9A* reaction products; Lane CK, control sample analyzed as above, except that no *nTaAA9A* was added.

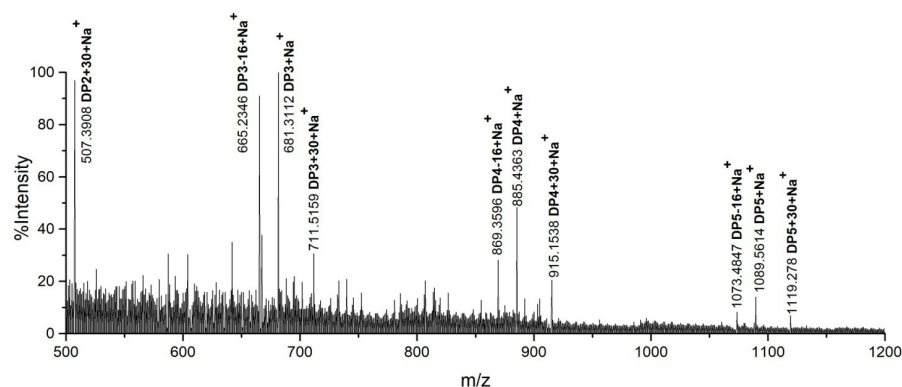


Figure 3. Identification of *nTaAA9A* permethylated reaction products using MALDI–TOF MS. *nTaAA9A* reaction products upon incubation of 0.5% PASC with *nTaAA9A* in 10 mM HOAc–NH₄OAc (pH 5.0) and 1 mM ascorbate at 50 °C for 48 h, followed by permethylation with methyl iodide. C1-oxidized oligosaccharides ($m/z +30$), C4-oxidized oligosaccharides ($m/z -16$), and non-oxidized oligosaccharides ($m/z +0$).

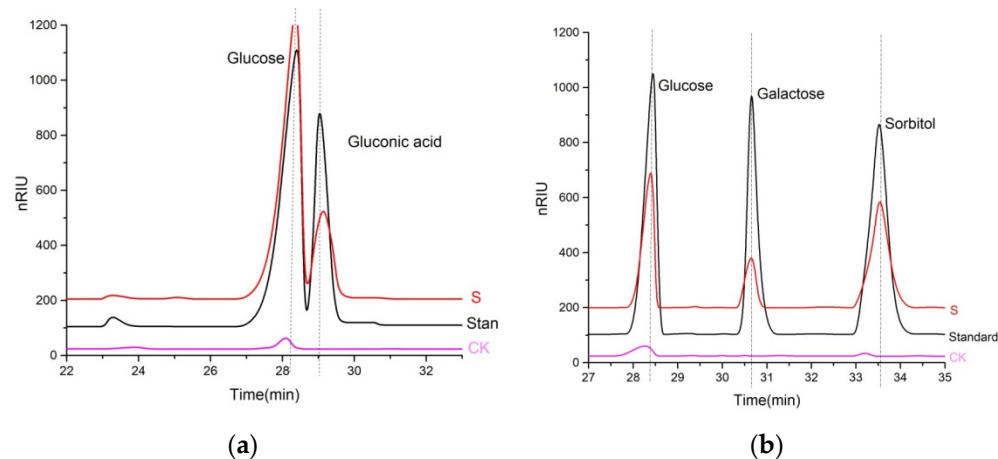


Figure 4. Identification of *nTaAA9A* reaction products using HPLC–RID. (a) *nTaAA9A* reaction products after incubation of 0.5% PASC with *TaAA9A* in 10 mM HOAc–NH₄OAc (pH 5.0) and 1 mM ascorbate at 50 °C for 48 h, followed by hydrolysis with TFA. C1-oxidized products, if present, were hydrolyzed by TFA to yield glucose and gluconic acid. The standard used was a mixture of glucose and gluconic acid; S: *nTaAA9A* reaction products hydrolyzed by TFA; CK, the control sample analyzed as above but without *nTaAA9A*. (b) *TaAA9A* reaction products upon incubation of 0.5% PASC with *TaAA9A* in 10 mM HOAc–NH₄OAc (pH 5.0) and 1 mM ascorbate at 50 °C for 48 h, followed by reduction with NaBH₄ and by hydrolysis with TFA. If there were C4-oxidized products, they were reduced by NaBH₄, followed by hydrolysis with TFA to yield glucose, galactose, and sorbitol. Standard, a mixture of glucose, galactose, and sorbitol; S: *nTaAA9A* reaction products reduced by NaBH₄, followed by hydrolysis with TFA; CK, the control sample was analyzed as above, except without *nTaAA9A*.

It has been demonstrated that *rTaAA9A* expressed in *Aspergillus oryzae* can cleave cellulose to produce C1- and C4-oxidized cello-oligosaccharides [17], using MALDI–TOF MS. In the present study, we show that the native *TaAA9A* can cleave cellulose to produce C1- and C4-oxidized cello-oligosaccharides using MALDI–TOF MS and HPLC–RID analysis, which further confirms the nature of the C1- and C4-oxidizing activity of *nTaAA9A*.

The activity of *nTaAA9A* towards xylan was also investigated. MALDI–TOF MS analysis of *nTaAA9A* reaction products with xylan as a substrate showed that *nTaAA9A* can cleave xylan to produce C1- and C4-oxidized xylo-oligosaccharides (Figures 5a,b and S2), similar to *LsAA9A* from *Lentinus similis* [12] and *MtLPMO9A* from *Myceliophthora ther-*

mophila [24]. Notably, *T. aurantiacus* can simultaneously secrete three main enzymes on biomass substrates: a GH7 cellobiohydrolase, a GH10 xylanase, and *TaAA9A*. These three enzymes have been shown to be key players in efficient biomass degradation [31]. It could, therefore, be suggested that *TaAA9A* may synergistically act with the GH10 xylanase on hemi-cellulose via both oxidative and hydrolytic mechanisms to enhance the degradation of hemi-cellulose [17].

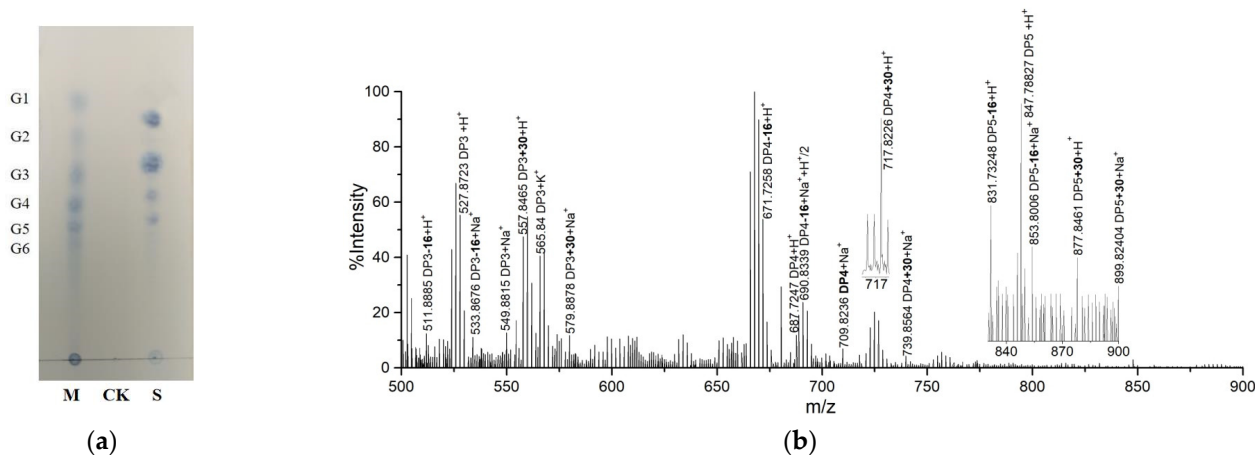


Figure 5. Identification of *nTaAA9A* permethylated reaction products with xylan as a substrate using TLC and MALDI-TOF MS. (a) TLC: *nTaAA9A* reaction products upon incubation of 0.5% xylan with *TaAA9A* in 10 mM HOAc-NH₄OAc (pH 5.0) and 1 mM ascorbate at 50 °C for 48 h. Lane M, standard cello-oligosaccharides (G1–G6); Lane S, *nTaAA9A* reaction products; Lane CK, control sample analyzed as above but without *nTaAA9A*. (b) MALDI-TOF MS: *nTaAA9A* reaction products after incubation of 0.5% xylan with *nTaAA9A* in 10 mM HOAc-NH₄OAc (pH 5.0) and 1 mM ascorbate at 50 °C for 48 h, followed by permethylation with methyl iodide. C1-oxidized xylo-oligosaccharides ($m/z +30$), C4-oxidized xylo-oligosaccharides ($m/z -16$), and non-oxidized xylo-oligosaccharides ($m/z +0$).

2.3. Structure Quality and Description

The structure of the native *TaAA9A* was determined to 1.36 Å resolution to final R_{work} and R_{free} of 0.151 and 0.185, respectively (Table 1). The final model contained 1762 protein atoms and 307 water molecules. The C-terminal Gly residue according to the amino acid sequence was not visible in the electron density map and thus, it was not modelled. Like other crystal structures of various LPMOs, *nTaAA9A* is characterized by a β -sandwich fold with two twisted antiparallel β -sheets connected through loops of various lengths and conformation. The active site is located on a flat solvent-exposed region of the molecule, in contrast to traditional cellulases that possess a substrate-binding cleft or tunnel. A Cu²⁺ ion involved in the catalytic reaction was identified at the N-terminal, as previously observed. The Cu²⁺ ion was refined to a temperature factor of 13.2 Å² and occupancy of 1.0, suggesting a well-defined tightly bound ion. His1, one of the Cu²⁺-coordinating residues, was found methylated, as also observed in other LPMO structures. The reason, in general, of this methylation in LPMOs is still unclear, although LPMOs that lack this post-translational modification are still catalytically active [17]. It has been suggested that His1 methylation may convey protection against oxidative damage [17,32]. This posttranslational modification is not always present and is not expected in LPMOs which are produced in *P. pastoris* [32], as for example in *MCAA9F* [21]. The final structure also contains two N-acetyl-glucosamine (NAG) molecules which were identified based on the electron-density map and built in Asn138.

Table 1. X-ray data collection and refinement statistics. Numbers in parentheses refer to the outermost resolution shell.

Data Collection	
Beamline	P13 (PETRA III, DESY)
Wavelength (Å)	0.9762
Resolution (Å)	44.63–1.36 (1.41–1.36)
Space group	$P2_12_12_1$
Unit cell <i>a</i> , <i>b</i> , <i>c</i> (Å)	37.7, 64.2, 88.5
No. of observations	559,476 (22,595)
No. of unique reflections	43,359 (2631)
Completeness (%)	92.7 (58.5)
Multiplicity	12.9 (8.6)
Mosaicity (°)	0.22
R_{meas}	0.218 (2.993)
$CC_{1/2}$	0.998 (0.251)
Wilson B factor (Å ²)	22.1
Refinement	
No. of reflections used	43,220
$R_{\text{cryst}}/R_{\text{free}}$	0.151/0.185
RMSD in bonds (Å)	0.005
RMSD in angles (°)	0.867
Number of protein atoms	1762
No. of water molecules	307
Average B-factor (Å ²)	17.6
Ramachandran favored/outliers (%)	99.1/0.0
Clashscore	2.54
PDB id	7q1k

2.4. Structural Comparison with rTaAA9A

Structural superposition resulted in a root-mean-square deviation (rmsd) of 0.43 Å between nTaAA9A and rTaAA9A, suggesting only subtle differences between the two structures. The highest deviations (~0.8–2.4 Å) were found in the regions 9–13, 25–30, 184–187, 202–203, and 213–217 (Figure 6). Also, in Asn138, owing to the different glycosylation in that residue. Asn138 was glycosylated with at least two NAG molecules, as found in the crystal structure. A third glycan was found, but the density was not enough to model it. In rTaAA9A, only one NAG molecule was attached after deglycosylation of the expressed rTaAA9A [17]. Close inspection revealed a different orientation for the side chain of Asn138 and, consequently, the position of the glycan moieties (Figure 7). In nTaAA9A, the two NAG molecules can sit in a shallow groove and make interactions with Asn13, Gln78, and Gln5. In contrast, the NAG molecule in rTaAA9A points outwards and is exposed to the solvent. The subtle changes in surface residues may contribute to the slightly different solvent-accessible area in the native and recombinant TaAA9A (9285 Å² and 9416 Å², respectively).

2.5. Oligosaccharide Binding

The TaAA9A structure provides insight into the molecular basis of cellulose C1 and C4 oxidation. TaAA9A has an active site containing a copper ion, which is coordinated by two highly conserved His residues (His1 and His86, known as a histidine brace) to create a copper ion-binding site and also a buried highly conserved Tyr residue (Tyr175) that occupies the axial position. Direct structural evidence of LPMO–substrate interaction in *Lentinus similis* AA9A and *Collariella virescens* AA9 in the presence of cellohexaose [33] has shown that the copper ion in the active site is close to the C1 and C4 carbon atoms of the oligosaccharides [12]. Superposition of TaAA9A onto CvAA9_A–cellohexaose (rmsd 0.9 Å for 133 equivalent residues; Figure S3) revealed that the active site of nTaAA9A was near to the C1 and C4 carbons of cellohexaose, supporting the C1 and C4 oxidation on cellulose by

TaAA9A (Figure 8). An important difference between *CvAA9_A*, *LsAA9A*, and *TaAA9A* is the presence of a long loop (residues 16–31) in the latter. Differences also in the length of the active loops were identified that may play a role in the orientation of the substrate. Individual residues could also affect binding as, for example, Leu41 could clash with the substrate, whereas in *CvAA9_A*, there is a shorter residue (Thr28). Arg164 belongs to a long external loop (157–164) and makes interactions with BGC-5. In *TaAA9A*, the equivalent loop is shorter, and interactions with glucose units to provide some stabilization in the binding are therefore not feasible. In general, different loop lengths in AA9s have been implicated in specificity for C1, C4, or C1/C4 oxidation. Tyr212, a highly conserved residue, makes stacking interactions with the flat pyranose ring of the substrate [34] and is likely to support substrate binding in a similar fashion in *TaAA9A* as well.

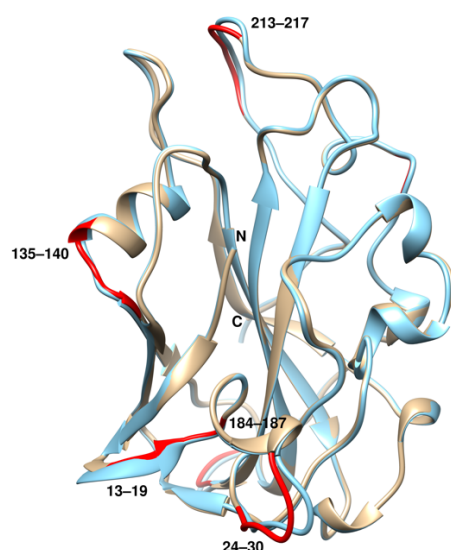


Figure 6. Structural comparison of *nTaAA9A* (brown) with *rTaAA9A* (cyan). The regions with the highest variations are indicated in red color and labelled.

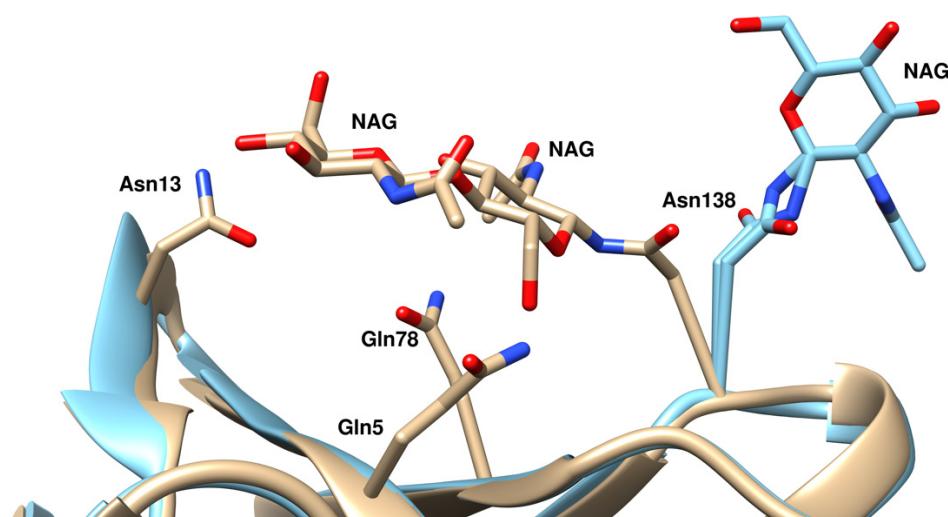


Figure 7. Glycosylation at Asn138. *nTaAA9A* is depicted in brown, and *rTaAA9A* in cyan.

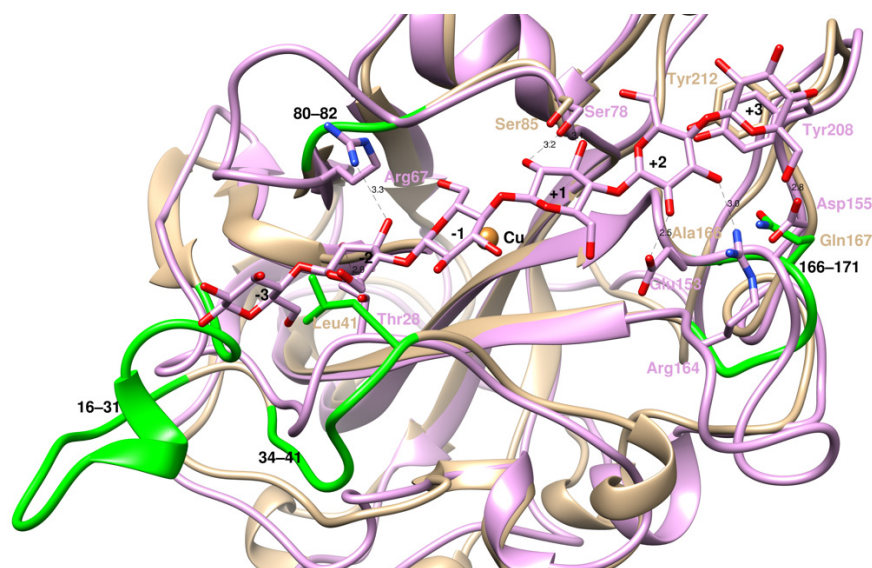


Figure 8. The active sites of *nTaAA9A* (brown) and *CvAA9_A* (pink; PDB id 6yde). Cellohexaose bound to *CvAA9_A* is shown in stick representation. *nTaAA9A* loops that show differences with corresponding loops in *CvAA9_A* are colored in green and labeled. The *CvAA9_A* residues that make hydrogen bond interactions with cellohexaose are shown as sticks and labelled. Tyr208 (Tyr212 in *nTaAA9A*) that provides additional stabilizing interactions with the oligosaccharide is also shown. The structural equivalent residues in *nTaAA9* are depicted and labeled. *CvAA9_A* residues Arg67 and Arg164 correspond to gaps in *nTaAA9A* (Figure S3), and no structural equivalent residues are shown.

The structural superposition also explains difficulties in obtaining structures of the complexes. Clashes with symmetry-related molecules in the crystal lattice usually obstruct ligand binding in LPMOs. Lattice problems have been identified in *rTaAA9A* crystals and have prevented crystallographic binding studies. Although the *nTaAA9* crystals reported here are different from those of the *rTaAA9A* (space group $P2_1$ and two molecules in the asymmetric unit), residues 68–71 and 182–184 of a symmetry-related *nTaAA9A* clash with three of the glucose moieties of the substrate, whereas the rest of the substrate makes no contacts with symmetry-related molecules.

2.6. Thermostability Properties

Theoretically, AA9 LPMOs from thermophilic fungi should be thermostable. In this study, the thermostability of *TaAA9A* was investigated by detecting gluconic acid in *TaAA9A* reaction products hydrolyzed with TFA, using HPLC–RID. The analysis revealed that *nTaAA9A* exhibits high thermostability (Figure 9), consistent with other thermostable enzymes from thermophilic fungi [35,36]. The enzyme retained about 84.3%, 63.7%, and 35.3% of its activity after incubation for 30 min at 60, 70, and 80 °C, respectively. A cluster of four residues (Val90, Ser131, Leu134, and Trp141; Figure S4) was previously identified in *TaAA9A* and used to create a thermostable variant of *AfuAA9A* [18]. The improvement in *AfuAA9A* thermostability was attributed to the elimination of some unfavorable electrostatic interactions in the enzyme.

Owing to the difficulties in quantitative activity determination of LPMOs, there are only a few reports of their thermostability using activity assay [18,33,37]. So far, the thermostability of only three LPMOs from non-thermophilic fungi, *AfuAA9A* from *Aspergillus fumigatus*, *LsAA9A* from *Lentinus similis*, and *TcAA9A* from *Talaromyces cellulolyticus*, have been measured using differential scanning fluorimetry, differential scanning calorimetry, and activity assay. *AfuAA9A* and *LsAA9A* exhibited a melting temperature T_m of 68–69 °C and thermal inflection, T_i , of 71.8 °C, respectively [33], whereas *TcAA9A* fully lost its activity after incubation at 50 °C for 8 h [37].

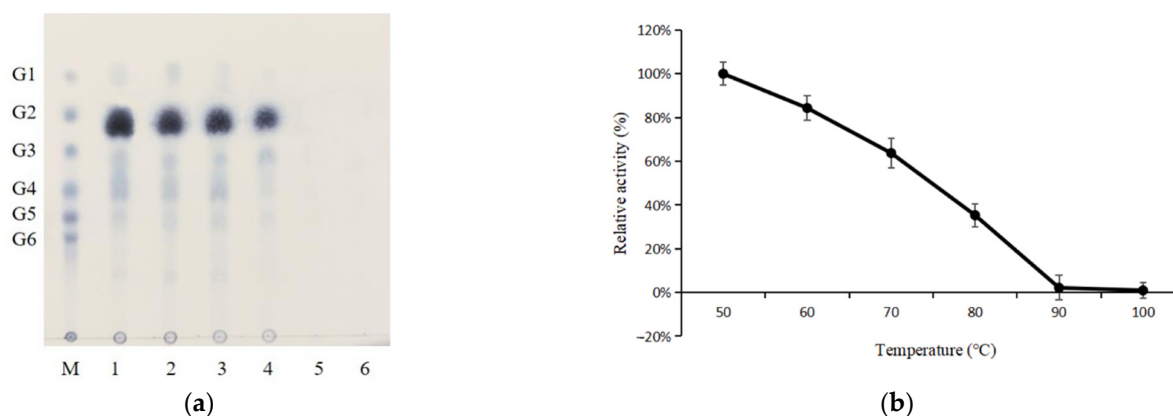


Figure 9. Determination of *nTaAA9A* thermostability. (a) TLC analysis of *nTaAA9A* reaction products. *nTaAA9A* was initially treated for 30 min at 50, 60, 70, 80, 90, and 100 °C (lanes 1–6, respectively; M: standard cello-oligosaccharides) in 10 mM $\text{NH}_4\text{OAc-HOAc}$ (pH 5.0) without substrate. The treated *nTaAA9A* was incubated with 0.5% PASC in 10 mM $\text{HOAc-NH}_4\text{OAc}$ (pH 5.0) and 1 mM ascorbate at 50 °C for 48 h. (b) Residual activity of *nTaAA9A* as a percentage of the maximum activity (100%). The residual *nTaAA9A* activities were measured using HPLC–RID by detecting gluconic acid in *nTaAA9A* reaction products after their hydrolysis with TFA. The experiment was carried out in triplicates.

Thermostability parameters, such as the number of charged residues, surface area, small-volume aliphatic amino acids, and salt bridges, which have been proposed as indicative of protein thermostability [38,39], are shown in Table 2. The thermostability, however, is sometimes a combination of different factors and not easily explained by a single parameter. In the absence of thermostability measurements for *McAA9F*, the temperature-dependent stability was calculated using the SCooP algorithm, a Gibbs–Helmholtz equation-based program [40] which calculates all the thermodynamic quantities associated with the two-fold transition of proteins (e.g., the melting temperature T_m , the standard folding enthalpy H_m measured at T_m , and the standard folding heat capacity C_p). Theoretical measurements were carried out for all enzymes. *TaAA9A* was found to have a higher T_m than *McAA9F*, although an accurate measurement of their thermostabilities would need experimental verification under similar assay conditions. Nevertheless, more studies are required to better understand the thermostability issues for this family of enzymes.

Table 2. Comparative statistics of thermostability parameters in AA9 LPMOs[#].

Parameter	<i>nTaAA9A</i>	<i>McAA9F</i> (7ntI)	<i>CvAA9_A</i> (6yde)	<i>AfuAA9A</i> (6h1z)	<i>LsAA9A</i> (5n04)	<i>TcAA9A</i> GenBank (GAM42970.1)
Asp + Glu (−) [#]	19	16	34	18	21	19
Arg + Lys (+)	7	7	24	10	10	9
Pro/Gly	0.84	1.04	0.91	0.57	1.11	0.76
Val (%)	5.3	4.1	8.7	4.4	9.8	10.3
Amino acid residues	228	222	252	229	235	246
SAS (Å ²)	9285.0	9034.0	9649.0	9363.0	9456	-
Intra-chain salt bridges [§]	3	2	3	3	11	-
Melting temperature T_m (°C) [‡]	56.1	49.4	57.5	57.8	51.6	-

[#] Amino acid calculations were carried out on ExPASy ProtParam (<https://web.expasy.org/protparam/> accessed on 20 November 2021). [§] Calculated with ESBRI (<http://bioinformatica.isa.cnr.it/ESBRI/introduction.html> accessed on 20 November 2021) [41]. [‡] Calculated with SCooP_v1.0 (<http://babylone.ulb.ac.be/SCooP> accessed on 20 November 2021) [40].

3. Materials and Methods

3.1. Strains and Chemicals

Thermoascus aurantiacus strain CGMCC3.17992 from fresh horse dung from China was isolated according to a method described previously [42]. It was deposited in the China

General Microbiological Culture Collection Center (CGMCC), a publicly accessible culture collection. A standard cello-oligosaccharide mixture was purchased from Elicityl (Crolles, France). Avicel PH-101, xylan, ascorbate (Vc), glucose, galactose, and gluconic acid were purchased from Sigma-Aldrich.

3.2. Purification and Identification of *nTaAA9A* from *Thermoascus aurantiacus*

The native secretory *TaAA9A* was purified from a *T. aurantiacus* culture grown at 50 °C for 7 days in cellulose-containing medium [43] supplemented with 0.1 mM CuSO₄. After the 7 days of incubation, the mycelium was initially filtered off, and the filtrate was subsequently centrifuged at 10,000× *g* for 15 min at 4 °C. The resultant supernatant was used for the purification. Ion-exchange chromatography on a DEAE-Sephacel column (GE Healthcare, Chicago, IL, USA) followed by gel filtration on an Enrich SEC650 column (BIO-RAD, Hercules, CA, USA) was employed. Solid ammonium sulphate was initially added to the resultant supernatant, leading to 90% saturation. After 6 h, the resulting precipitate was collected by centrifugation at 10,000× *g* for 15 min at 4 °C, dissolved, and dialyzed in 50 mM Tris-HCl (pH 8.0) (buffer A). In the subsequent step, the dialyzed sample was loaded on a DEAE-Sephacel column equilibrated with buffer A. *nTaAA9A* was eluted with a 120 mL linear gradient of NaCl (0–0.3 M in buffer A) at a flow rate of 2 mL/min. Fractions with enzymatic activity were pooled and concentrated by vacuum freeze-drying. In the last step, 0.25 mL of the concentrated sample was applied to a gel filtration Enrich SEC650 column. *nTaAA9A* was eluted with 50 mL of buffer A at a flow rate of 0.5 mL/min. The purified *nTaAA9A* was visualized on an SDS-PAGE gel, and the band of interest was cut out. The amino acid sequence of the excised *nTaAA9A* protein band was determined using LC-MS/MS according to a method previously described [30]. All data were analyzed using MASCOT 2.2 software (Matrix Science). MS/MS spectra were searched against the *TaAA9A* (ACS05720.1) protein sequence database [17].

3.3. Protein Determination, SDS-PAGE, and Carbohydrate Staining

Protein concentration was measured with the Lowry method [44]. The purity of the *nTaAA9A* protein was assessed using SDS-PAGE [45]. The carbohydrates in the *nTaAA9A* enzyme were stained with the Pierce™ Glycoprotein Staining Kit (Thermo Scientific, Waltham, MA, USA).

3.4. *nTaAA9A* Activity Assay

Phosphoric acid-swollen cellulose (PASC) was prepared as described by Phillips et al. [46]. Activity assays, including the use of xylan as a substrate, were carried out as previously described [43]. *nTaAA9A* reaction products were identified using TLC, matrix-assisted laser desorption-ionization-time-of-flight mass spectrometry (MALDI-TOF MS), and HPLC-RID analysis.

3.5. TLC and MALDI-TOF MS

Thin-layer chromatography (TLC) was used to analyze *nTaAA9A* reaction products according to a method previously described [43]. *nTaAA9A* reaction products were further analyzed using MALDI-TOF MS as described in previous publications [30,43].

3.6. Permethylated and Reduced *nTaAA9A* Reaction Products

Permethylation of *nTaAA9A* reaction products was carried out as described [47], and reduction of *TaAA9A* reaction products was carried out as previously described [22].

3.7. HPLC-RID

nTaAA9A reaction products and their reduced reaction products were hydrolyzed by TFA as previously described [22] and analyzed by HPLC-RID using an Agilent 1200 series instrument with a refractive index detector (RID). Products were separated using an Aminex HPX-87H column (Bio-Rad) and a 5 mM H₂SO₄ mobile phase. Glucose, sorbitol, and

gluconic acid were annotated based on the elution pattern of standard glucose, sorbitol, and gluconic acid solutions. The flow rate was 0.2 mL/min, and the column was maintained at a temperature of 30 °C.

3.8. Protein Crystallization

The protein was concentrated to ~10 mg/mL in buffer NaOAc 10 mM, NaN₃ 0.002%, pH 4.8. Crystals were produced at 16 °C using the vapor-diffusion hanging drop method with a well solution of 0.2 M ammonium sulfate, 0.1 M HEPES-NaOH pH 7.5, 25% *w/v* PEG 3350. The drops consisted of 2 µL of protein solution mixed with 2 µL of the well solution. Crystals appeared after ~3 days, most of them in clusters. For crystallographic data collection, single crystals were carefully separated from the clusters.

3.9. Structure Determination and Validation

X-ray diffraction data were collected at cryogenic temperatures (100 K) in the presence of 10% *v/v* glycerol as cryoprotectant. Data to 1.86 Å resolution were initially collected at ESRF (Grenoble, France), and the resolution was later extended to 1.36 Å using X-ray data collected at EMBL-Hamburg (beamline P13 at the PETRA III ring). Data processing was carried out with XDS [48], followed by scaling with AIMLESS [49]. Initial phases were obtained with molecular replacement using the structure of rTaAA9A (PDB id 2yet) as search model, leading to a single solution with TFZ = 33.8 in Phaser [50]. Refinement was carried out with PHENIX (v. 1.19.2) [51] using maximum likelihood as the target and simulated annealing with a starting temperature of 1000 K. Water was added at the final stages when the R_{free} (calculated using 5% of the data excluded from the refinement) dropped below 30%. The electron difference maps were examined, and a glycosylation site was identified at Asn138 based on the electron density difference map. Validation of the structure was performed with Molprobity [52] and validation tools in Coot [53]. Figures of the structures were created with Chimera [54].

4. Conclusions

In the present study, a native thermostable AA9 LPMO, nTaAA9A, from the thermophilic fungus *T. aurantiacus* was purified and characterized. nTaAA9A was active and exhibited C1- and C4-oxidizing activity against cellulose and xylan. The enzyme was found to retain significant activity at elevated temperatures. The purified enzyme was found to have a single glycosylation site with at least two NAG molecules. Structural differences were identified with the recombinant rTaAA9A in surface loops and in the glycosylation site. The results will help in exploiting TaAA9A in various biotechnological applications to improve the cleavage of cellulose and xylan.

Supplementary Materials: The following supporting information can be downloaded at: <https://www.mdpi.com/article/10.3390/catal12020139/s1>, Figure S1: Identification of TaAA9A using LC-MS; Figure S2: Chemical structures of oxidized and non-oxidized xylo-oligosaccharides; Figure S3: Structure-based sequence alignment of nTaAA9A and CvAA9_A; Figure S4: Depiction of the four-residue cluster used for thermostability improvement.

Author Contributions: A.C.P., D.L. designed the experiments. W.Y., I.M. performed the experiments. A.C.P., D.L., W.Y., I.M. analyzed the data. A.C.P., D.L. contributed to the drafting and revision of the manuscript. All authors have read and agreed to the published version of the manuscript.

Funding: This research was funded by the National Natural Science Foundation of China (Grant No. 31571949) and the Ministry of Science and Technology of China (Grant No. 2015BAD15B05).

Data Availability Statement: All data generated or analyzed during this study are included in this published article.

Acknowledgments: We thank Biocenter Finland for instrument support and the staff at the P13 beamline (EMBL-Hamburg, DESY) for help during data collection. Access to synchrotron beamtime

was provided by the European Union's Horizon 2020 iNEXT-Discovery programme (grant agreement No 871037).

Conflicts of Interest: The authors declare no conflict of interest.

References

1. Service, R.F. Is there a road ahead for cellulosic ethanol? *Science* **2010**, *329*, 784–785. [[CrossRef](#)]
2. Vaaje-Kolstad, G.; Westereng, B.; Horn, S.J.; Liu, Z.; Zhai, H.; Sørlie, M.; Eijsink, V.G.H. An Oxidative Enzyme Boosting the Enzymatic Conversion of Recalcitrant Polysaccharides. *Science* **2010**, *330*, 219–222. [[CrossRef](#)] [[PubMed](#)]
3. Vaaje-Kolstad, G.; Forsberg, Z.; Loose, J.S.; Bissaro, B.; Eijsink, V.G. Structural diversity of lytic polysaccharide monoxygenases. *Curr. Opin. Struct. Biol.* **2017**, *44*, 67–76. [[CrossRef](#)]
4. Bissaro, B.; Várnai, A.; Røhr, Å.K.; Eijsink, V.G.H. Oxidoreductases and Reactive Oxygen Species in Conversion of Lignocellulosic Biomass. *Microbiol. Mol. Biol. Rev.* **2018**, *82*, e00029-18. [[CrossRef](#)] [[PubMed](#)]
5. Levasseur, A.; Drula, E.; Lombard, V.; Coutinho, P.M.; Henrissat, B. Expansion of the enzymatic repertoire of the CAZy database to integrate auxiliary redox enzymes. *Biotechnol. Biofuels* **2013**, *6*, 41. [[CrossRef](#)] [[PubMed](#)]
6. Forsberg, Z.; Sørlie, M.; Petrović, D.; Courtade, G.; Aachmann, F.L.; Vaaje-Kolstad, G.; Bissaro, B.; Røhr, Å.K.; Eijsink, V.G. Polysaccharide degradation by lytic polysaccharide monoxygenases. *Curr. Opin. Struct. Biol.* **2019**, *59*, 54–64. [[CrossRef](#)]
7. Tamburrini, K.C.; Terrapon, N.; Lombard, V.; Bissaro, B.; Longhi, S.; Berrin, J.-G. Bioinformatic Analysis of Lytic Polysaccharide Monoxygenases Reveals the Pan-Families Occurrence of Intrinsically Disordered C-Terminal Extensions. *Biomolecules* **2021**, *11*, 1632. [[CrossRef](#)]
8. Chylenski, P.; Bissaro, B.; Sørlie, M.; Røhr, Å.K.; Várnai, A.; Horn, S.J.; Eijsink, V.G.H. Lytic Polysaccharide Monoxygenases in Enzymatic Processing of Lignocellulosic Biomass. *ACS Catal.* **2019**, *9*, 4970–4991. [[CrossRef](#)]
9. Tandrup, T.; Frandsen, K.E.H.; Johansen, K.S.; Berrin, J.-G.; Leggio, L.L. Recent insights into lytic polysaccharide monoxygenases (LPMOs). *Biochem. Soc. Trans.* **2018**, *46*, 1431–1447. [[CrossRef](#)]
10. Askarian, F.; Uchiyama, S.; Masson, H.; Sørensen, H.V.; Golten, O.; Bunæs, A.C.; Mekasha, S.; Røhr, Å.K.; Kommedal, E.; Ludviksen, J.A.; et al. The lytic polysaccharide monoxygenase CbpD promotes *Pseudomonas aeruginosa* virulence in systemic infection. *Nat. Commun.* **2021**, *12*, 1230. [[CrossRef](#)]
11. Chiu, E.; Hijnen, M.; Bunker, R.D.; Boudes, M.; Rajendran, C.; Aizel, K.; Olieric, V.; Schulze-Briese, C.; Mitsuhashi, W.; Young, V.; et al. Structural basis for the enhancement of virulence by viral spindles and their in vivo crystallization. *Proc. Natl. Acad. Sci. USA* **2015**, *112*, 3973–3978. [[CrossRef](#)] [[PubMed](#)]
12. Simmons, T.J.; Frandsen, K.E.H.; Ciano, L.; Tryfona, T.; Lenfant, N.; Poulsen, J.C.; Wilson, L.F.L.; Tandrup, T.; Tovborg, M.; Schnorr, K.; et al. Structural and electronic determinants of lytic polysaccharide monoxygenase reactivity on polysaccharide substrates. *Nat. Commun.* **2017**, *8*, 1064. [[CrossRef](#)] [[PubMed](#)]
13. Wang, B.; Johnston, E.M.; Li, P.; Shaik, S.; Davies, G.J.; Walton, P.H.; Rovira, C. QM/MM Studies into the H₂O₂-Dependent Activity of Lytic Polysaccharide Monoxygenases: Evidence for the Formation of a Caged Hydroxyl Radical Intermediate. *ACS Catal.* **2018**, *8*, 1346–1351. [[CrossRef](#)]
14. Wang, B.; Walton, P.H.; Rovira, C. Molecular Mechanisms of Oxygen Activation and Hydrogen Peroxide Formation in Lytic Polysaccharide Monoxygenases. *ACS Catal.* **2019**, *9*, 4958–4969. [[CrossRef](#)]
15. Paradisi, A.; Johnston, E.M.; Tovborg, M.; Nicoll, C.R.; Ciano, L.; Dowle, A.; McMaster, J.; Hancock, Y.; Davies, G.J.; Walton, P.H. Formation of a Copper(II)–Tyrosyl Complex at the Active Site of Lytic Polysaccharide Monoxygenases Following Oxidation by H₂O₂. *J. Am. Chem. Soc.* **2019**, *141*, 18585–18599. [[CrossRef](#)]
16. Frandsen, K.E.H.; Leggio, L.L. Lytic polysaccharide monoxygenases: A crystallographer's view on a new class of biomass-degrading enzymes. *IUCr* **2016**, *3*, 448–467. [[CrossRef](#)]
17. Quinlan, R.J.; Sweeney, M.D.; Leggio, L.L.; Otten, H.; Poulsen, J.-C.N.; Johansen, K.S.; Krogh, K.B.R.M.; Jørgensen, C.I.; Tovborg, M.; Anthonsen, A.; et al. Insights into the oxidative degradation of cellulose by a copper metalloenzyme that exploits biomass components. *Proc. Natl. Acad. Sci. USA* **2011**, *108*, 15079–15084. [[CrossRef](#)]
18. Leggio, L.L.; Weihe, C.D.; Poulsen, J.-C.N.; Sweeney, M.; Rasmussen, F.; Lin, J.; De Maria, L.; Wogulis, M. Structure of a lytic polysaccharide monoxygenase from *Aspergillus fumigatus* and an engineered thermostable variant. *Carbohydr. Res.* **2018**, *469*, 55–59. [[CrossRef](#)]
19. Bissaro, B.; Isaksen, I.; Vaaje-Kolstad, G.; Eijsink, V.G.H.; Røhr, Å.K. How a Lytic Polysaccharide Monoxygenase Binds Crystalline Chitin. *Biochemistry* **2018**, *57*, 1893–1906. [[CrossRef](#)]
20. Leggio, L.L.; Simmons, T.J.; Poulsen, J.-C.N.; Frandsen, K.E.H.; Hemsworth, G.R.; Stringer, M.A.; von Freiesleben, P.; Tovborg, M.; Johansen, K.S.; De Maria, L.; et al. Structure and boosting activity of a starch-degrading lytic polysaccharide monoxygenase. *Nat. Commun.* **2015**, *6*, 5961. [[CrossRef](#)]
21. Mazurkewich, S.; Seveso, A.; Hüttner, S.; Brändén, G.; Larsbrink, J. Structure of a C1/C4-oxidizing AA9 lytic polysaccharide monoxygenase from the thermophilic fungus *Malbranchea cinnamomea*. *Acta Crystallogr. Sect. D Struct. Biol.* **2021**, *D77*, 1019–1026. [[CrossRef](#)] [[PubMed](#)]
22. Beeson, W.T.; Phillips, C.M.; Cate, J.H.D.; Marletta, M.A. Oxidative Cleavage of Cellulose by Fungal Copper-Dependent Polysaccharide Monoxygenases. *J. Am. Chem. Soc.* **2012**, *134*, 890–892. [[CrossRef](#)] [[PubMed](#)]

23. Bey, M.; Zhou, S.; Poidevin, L.; Henrissat, B.; Coutinho, P.M.; Berrin, J.-G.; Sigoillot, J.-C. Cello-Oligosaccharide Oxidation Reveals Differences between Two Lytic Polysaccharide Monooxygenases (Family GH61) from *Podospora anserina*. *Appl. Environ. Microbiol.* **2013**, *79*, 488–496. [[CrossRef](#)] [[PubMed](#)]
24. Frommhagen, M.; Sforza, S.; Westphal, A.H.; Visser, J.; Hinz, S.W.A.; Koetsier, M.J.; Van Berkel, W.J.H.; Gruppen, H.; Kabel, M.A. Discovery of the combined oxidative cleavage of plant xylan and cellulose by a new fungal polysaccharide monooxygenase. *Biotechnol. Biofuels* **2015**, *8*, 101. [[CrossRef](#)] [[PubMed](#)]
25. Zerva, A.; Pentari, C.; Grisel, S.; Berrin, J.-G.; Topakas, E. A new synergistic relationship between xylan-active LPMO and xylobiohydrolase to tackle recalcitrant xylan. *Biotechnol. Biofuels* **2020**, *13*, 142. [[CrossRef](#)]
26. Lange, L.; Huang, Y.; Busk, P.K. Microbial decomposition of keratin in nature—A new hypothesis of industrial relevance. *Appl. Microbiol. Biotechnol.* **2016**, *100*, 2083–2096. [[CrossRef](#)]
27. Vu, V.V.; Beeson, W.T.; Phillips, C.M.; Cate, J.H.D.; Marletta, M.A. Determinants of Regioselective Hydroxylation in the Fungal Polysaccharide Monooxygenases. *J. Am. Chem. Soc.* **2014**, *136*, 562–565. [[CrossRef](#)]
28. Berka, R.M.; Grigoriev, I.V.; Otiillar, R.; Salamov, A.; Grimwood, J.; Reid, I.; Ishmael, N.; John, T.; Darmond, C.; Moisan, M.-C.; et al. Comparative genomic analysis of the thermophilic biomass-degrading fungi *Myceliophthora thermophila* and *Thielavia terrestris*. *Nat. Biotechnol.* **2011**, *29*, 922–927. [[CrossRef](#)]
29. Petrović, D.M.; Várnai, A.; Dimarogona, M.; Mathiesen, G.; Sandgren, M.; Westereng, B.; Eijsink, V.G.H. Comparison of three seemingly similar lytic polysaccharide monooxygenases from *Neurospora crassa* suggests different roles in plant biomass degradation. *J. Biol. Chem.* **2019**, *294*, 15068–15081. [[CrossRef](#)]
30. Chen, J.; Guo, X.; Zhu, M.; Chen, C.; Li, D. Polysaccharide monooxygenase-catalyzed oxidation of cellulose to glucuronic acid-containing cello-oligosaccharides. *Biotechnol. Biofuels* **2019**, *12*, 42. [[CrossRef](#)]
31. McClendon, S.D.; Batth, T.; Petzold, C.J.; Adams, P.D.; Simmons, B.A.; Singer, S.W. *Thermoascus aurantiacus* is a promising source of enzymes for biomass deconstruction under thermophilic conditions. *Biotechnol. Biofuels* **2012**, *5*, 54. [[CrossRef](#)] [[PubMed](#)]
32. Petrović, D.M.; Bissaro, B.; Chylenski, P.; Skaugen, M.; Sørli, M.; Jensen, M.S.; Aachmann, F.L.; Courtade, G.; Várnai, A.; Eijsink, V.G.H. Methylation of the N-terminal histidine protects a lytic polysaccharide monooxygenase from auto-oxidative inactivation. *Protein Sci.* **2018**, *27*, 1636–1650. [[CrossRef](#)] [[PubMed](#)]
33. Tandrup, T.; Tryfona, T.; Frandsen, K.E.H.; Johansen, K.S.; DuPree, P.; Leggio, L.L. Oligosaccharide Binding and Thermostability of Two Related AA9 Lytic Polysaccharide Monooxygenases. *Biochemistry* **2020**, *59*, 3347–3358. [[CrossRef](#)] [[PubMed](#)]
34. Harris, P.V.; Welner, D.; McFarland, K.C.; Re, E.; Poulsen, J.-C.N.; Brown, K.; Salbo, R.; Ding, H.; Vlasenko, E.; Merino, S.; et al. Stimulation of Lignocellulosic Biomass Hydrolysis by Proteins of Glycoside Hydrolase Family 61: Structure and Function of a Large, Enigmatic Family. *Biochemistry* **2010**, *49*, 3305–3316. [[CrossRef](#)] [[PubMed](#)]
35. Maheshwari, R.; Bharadwaj, G.; Bhat, M.K. Thermophilic Fungi: Their Physiology and Enzymes. *Microbiol. Mol. Biol. Rev.* **2000**, *64*, 461–488. [[CrossRef](#)]
36. Li, D.-C.; Li, A.-N.; Papageorgiou, A.C. Cellulases from Thermophilic Fungi: Recent Insights and Biotechnological Potential. *Enzym. Res.* **2011**, *2011*, 308730. [[CrossRef](#)]
37. Zhang, R.; Liu, Y.; Zhang, Y.; Feng, D.; Hou, S.; Guo, W.; Niu, K.; Jiang, Y.; Han, L.; Sindhu, L.; et al. Identification of a thermostable fungal lytic polysaccharide monooxygenase and evaluation of its effect on lignocellulosic degradation. *Appl. Microbiol. Biotechnol.* **2019**, *103*, 5739–5750. [[CrossRef](#)]
38. Panja, A.S.; Bandopadhyay, B.; Maiti, S. Protein Thermostability Is Owing to Their Preferences to Non-Polar Smaller Volume Amino Acids, Variations in Residual Physico-Chemical Properties and More Salt-Bridges. *PLoS ONE* **2015**, *10*, e0131495. [[CrossRef](#)]
39. Trivedi, S.; Gehlot, H.S.; Rao, S.R. Protein thermostability in Archaea and Eubacteria. *Genet. Mol. Res.* **2006**, *5*, 816–827.
40. Pucci, F.; Kwasiogoch, J.M.; Rooman, M. SCooP: An accurate and fast predictor of protein stability curves as a function of temperature. *Bioinformatics* **2017**, *33*, 3415–3422. [[CrossRef](#)]
41. Costantini, S.; Colonna, G.; Facchiano, A.M. ESBRI: A web server for evaluating salt bridges in proteins. *Bioinformatics* **2008**, *3*, 137–138. [[CrossRef](#)] [[PubMed](#)]
42. Li, D.-C.; Lu, M.; Li, Y.-L.; Lu, J. Purification and characterization of an endocellulase from the thermophilic fungus *Chaetomium thermophilum* CT2. *Enzym. Microb. Technol.* **2003**, *33*, 932–937. [[CrossRef](#)]
43. Chen, C.; Chen, J.; Geng, Z.; Wang, M.; Liu, N.; Li, D. Regioselectivity of oxidation by a polysaccharide monooxygenase from *Chaetomium thermophilum*. *Biotechnol. Biofuels* **2018**, *11*, 155. [[CrossRef](#)] [[PubMed](#)]
44. Lowry, O.H.; Rosebrough, N.J.; Farr, A.L.; Randall, R.J. Protein measurement with the Folin phenol reagent. *J. Biol. Chem.* **1951**, *193*, 265–275. [[CrossRef](#)]
45. Laemmli, U.K. Cleavage of Structural Proteins during the Assembly of the Head of Bacteriophage T4. *Nature* **1970**, *227*, 680–685. [[CrossRef](#)] [[PubMed](#)]
46. Phillips, C.M.; Beeson, W.T.; Cate, J.H.; Marletta, M.A. Cellobiose Dehydrogenase and a Copper-Dependent Polysaccharide Monooxygenase Potentiate Cellulose Degradation by *Neurospora crassa*. *ACS Chem. Biol.* **2011**, *6*, 1399–1406. [[CrossRef](#)]
47. Needs, P.W.; Selvendran, R.R. Avoiding oxidative degradation during sodium hydroxide/methyl iodide-mediated carbohydrate methylation in dimethyl sulfoxide. *Carbohydr. Res.* **1993**, *245*, 1–10. [[CrossRef](#)]
48. Kabsch, W. XDS. *Acta Crystallogr. Sect. D Struct. Biol.* **2010**, *D66*, 125–132. [[CrossRef](#)]
49. Evans, P.R.; Murshudov, G.N. How good are my data and what is the resolution? *Acta Crystallogr. Sect. D Struct. Biol.* **2013**, *D69*, 1204–1214. [[CrossRef](#)]

50. McCoy, A.J.; Grosse-Kunstleve, R.W.; Adams, P.D.; Winn, M.D.; Storoni, L.C.; Read, R.J. Phaser crystallographic software. *J. Appl. Crystallogr.* **2007**, *40*, 658–674. [[CrossRef](#)]
51. Adams, P.D.; Afonine, P.V.; Bunkóczy, G.; Chen, V.B.; Davis, I.W.; Echols, N.; Headd, J.J.; Hung, L.-W.; Kapral, G.J.; Grosse-Kunstleve, R.W.; et al. PHENIX: A comprehensive Python-based system for macromolecular structure solution. *Acta Crystallogr. Sect. D Struct. Biol.* **2010**, *D66*, 213–221. [[CrossRef](#)]
52. Chen, V.B.; Arendall, W.B., III; Headd, J.J.; Keedy, D.A.; Immormino, R.M.; Kapral, G.J.; Murray, L.W.; Richardson, J.S.; Richardson, D.C. MolProbity: All-atom structure validation for macromolecular crystallography. *Acta Crystallogr. Sect. D Struct. Biol.* **2010**, *D66*, 12–21. [[CrossRef](#)] [[PubMed](#)]
53. Emsley, P.; Cowtan, K. Coot: Model-building tools for molecular graphics. *Acta Crystallogr. Sect. D Struct. Biol.* **2004**, *D60*, 2126–2132. [[CrossRef](#)] [[PubMed](#)]
54. Pettersen, E.F.; Goddard, T.D.; Huang, C.C.; Couch, G.S.; Greenblatt, D.M.; Meng, E.C.; Ferrin, T.E. UCSF Chimera—A visualization system for exploratory research and analysis. *J. Comput. Chem.* **2004**, *25*, 1605–1612. [[CrossRef](#)] [[PubMed](#)]